

# Chopped Cold Neutron Beam Activation Analysis

Danyal J. Turkoglu<sup>1</sup> and H. Heather Chen-Mayer<sup>2</sup>, *Member, IEEE*

**Abstract**—A linear fast neutron beam chopper has been deployed at a prompt gamma activation analysis instrument, enabling in-beam activation analysis of short-lived ( $T_{1/2} > \sim 10$  ms) neutron capture products without the need for sample transfer. This article describes the design and operation of the chopper system and measurement results from test samples containing Se-77 ( $T_{1/2} = 17.36$  s) and Yb-175m ( $T_{1/2} = 0.0682$  s). The chopper timing was optimized for a specific isotope in each measurement, demonstrating an advantage of the programmable system. The linear response of the total gated counts in the decay phase to the incremented Se and Yb masses demonstrates the suitability of the system for quantitative analysis. Theoretical calculations based on the experimental parameters were in good agreement with the observed results. An example that illustrates the separation of overlapping energy peaks by the use of time-stamped list mode data acquisition is shown in a sample containing Yb-175m and Dy-165 ( $T_{1/2} = 75.4$  s).

**Index Terms**—Chopped neutron beam, linear chopper, neutron activation analysis, short-lived activation product.

## I. INTRODUCTION

NEUTRON activation analysis has two principal modes for observing the analytical signal generated through neutron capture in an unknown sample: instrumental neutron activation analysis (INAA) and prompt gamma activation analysis (PGAA). Both PGAA and INAA can be used to quantitatively determine mass fractions of suitable elements either by converting count rates to mass by the gamma ray cross section and detector efficiency or by comparison to standards.

INAA involves measuring the “delayed” gamma rays from radioisotope product that typically undergoes  $\beta^-$ ,  $\gamma$  decay cascades. Traditionally, INAA requires sample irradiation to occur inside the reactor, and the sample needs to be transferred to the laboratory for decay counting. Very short-lived radionuclides (half-lives of 100 s or less) pose unique measurement challenges which have inspired the development of cyclic activation methods [1]–[7], with repeat cycles of irradiation transfer counting, to address issues associated with the rapid decay of count rates, sample transfer, and detector dead time.

Manuscript received April 7, 2021; revised May 4, 2021; accepted May 11, 2021. Date of publication May 17, 2021; date of current version July 16, 2021.

Danyal J. Turkoglu was with the Center for Neutron Research, National Institute of Standards and Technology, Gaithersburg, MD 20899 USA. He is now with USNC-Tech, Seattle, WA 98199 USA (e-mail: d.turkoglu@usnc-tech.com).

H. Heather Chen-Mayer is with the Materials Measurement Laboratory, National Institute of Standards and Technology, Gaithersburg, MD 20899 USA (e-mail: chen-mayer@nist.gov).

Color versions of one or more figures in this article are available at <https://doi.org/10.1109/TNS.2021.3080682>.

Digital Object Identifier 10.1109/TNS.2021.3080682

The time required for sample transfer limits the utility for very short-lived nuclides.

PGAA [8] measures “prompt” gamma rays emitted in the rapid cascade decay of highly excited nuclear states after neutron capture ( $n, \gamma$ ) reaction. In contrast to INAA, PGAA is performed with a neutron beam outside the reactor, and the measurement is performed *in situ*, that is, measurement is performed where the sample is being irradiated. This provides a mechanism for performing INAA *in situ*, if the neutron beam can be pulsed. Pulses of neutrons periodically irradiate the target sample, creating “ON–OFF” states. During the beam-ON phase, the irradiated sample produces both prompt and delayed gamma rays, whereas during the beam-OFF phase, only the delayed gamma rays are emitted. By eliminating the need for sample transfer, nuclides with half-lives from milliseconds to tens of seconds can be measured, providing a capability currently relying on ultrafast transport systems that are only available in a few limited facilities worldwide.

This form of INAA has been demonstrated using a rotating disk shutter to deliver a pulsed neutron beam [9]–[11]. However, without more sophisticated phase modulation, a single rotating shutter has a fixed beam ON/OFF ratio predetermined by the width of the slit opening and the corresponding circumference of the disk that blocks the beam. This ratio remains constant regardless of the rotation frequency that governs the length of irradiation periods. This inflexibility prevents optimization of the system for a given analytical task. Therefore, we undertook the development of a linear shutter technology that permitted independent open and closed times as needed by the analytical requirements. The detector electronics are controlled by the timing of the chopper’s phase, recording the prompt and decay signals into separate channels. We term this new measurement method “chopped beam neutron activation analysis” (CBNAA), which can perform PGAA and INAA by time discrimination in a single setting. Although a programmable beam shutter has been demonstrated [12], the shortest irradiation period demonstrated is about 1 min, leaving room for improvement. This article reports on the construction and implementation of a programmable variable speed linear chopper system with a 40-ms transition time—the fastest among this class of choppers—pushing down the lower bound of accessible short-lived activation products.

## II. THEORY

The rate of production of gamma rays, ( $dN/dt$ ), with gamma ray energy  $E_g$  is given by (1) for the case with constant neutron beam flux  $\phi_0$  (i.e., self-shielding is negligible). Here,

$N_0$  is the number of target nuclei,  $\sigma_\gamma(E_\gamma)$  is the partial gamma ray production cross section, and  $\lambda$  is the decay constant, defined as  $\lambda = (\ln 2/T_{1/2})$ , where  $T_{1/2}$  is the half-life of the decay isotope

$$dN/dt = \varphi_0 N_0 \sigma_\gamma(E_\gamma) - \lambda N. \quad (1)$$

When the shutter closes, production of the activation product  $N$  ceases and it begins to decay away at a rate given by the following equation:

$$dN/dt = -\lambda N. \quad (2)$$

The analytical solutions to these differential equations are well-known. Defining the event rate, or activity, as  $A = -\lambda N$ , the solution to (1) can be written as follows:

$$A(t) = \varphi_0 N_0 \sigma_\gamma(E_\gamma) (1 - e^{-\lambda t}) = A_0 (1 - e^{-\lambda t}). \quad (3)$$

For irradiation time  $t = t_i \gg T_{1/2}$ , the activity reaches its saturation rate,  $A_0$ , since the production rate equals the decay rate. Note that this is immediately the case for prompt gammas that are emitted “instantaneously” after neutron capture. The activity is 99.9% of the saturation activity after  $t_i = 10T_{1/2}$ . The activity present at the end of irradiation,  $A(t_i) = A_0(1 - e^{-\lambda t_i})$ , further decays away exponentially as a function of time. The remaining activity after a cycle of  $t_i + t_d$  is

$$A(t_i + t_d) = A_0 (1 - e^{-\lambda t_i}) e^{-\lambda t_d} \quad (4)$$

where  $t_d$  is the time of decay. Following these relationships in a typical INAA measurement for best acceptable performance counting, decay and measurement times are selected that closely relate to the half-life of the nuclide of interest. Thus, high throughput can be achieved with assays involving short-lived nuclides.

The cycle time,  $T$ , is given by

$$T = t_i + t_w + t_d + t'_w \quad (5)$$

where  $t_w$  is the time between the end of irradiation and start of counting and  $t'_w$  is the time between the end of counting and start of irradiation. If  $t_w$  and  $t'_w$  are negligible compared with the half-life  $T_{1/2}$  for the activation product of interest, the cumulative detector response during counting is maximized when  $t_i = t_d = T_{1/2}$  [8]. The assumption that  $t_w$  and  $t'_w$  being negligible is more likely to be true in the case of CBNA, where the chopper transition time is 40 ms, whereas in cyclic INAA the transition time is in seconds. With CBNA, the half-life as short as 20.18 ms ( $^{24}\text{mNa}$ ) has been shown to be measurable.

We consider irradiation and counting times in terms of the half-life,  $T_{1/2}$ , of the activation product of interest so that the theoretical discussion that follows applies generally as long as  $t_w$  and  $t'_w$  can be neglected. Fig. 1 plots the fraction of saturation activity,  $F$ , as a function of half-lives into the measurement for the following combinations of  $(t_i, t_d)$  in multiples of  $T_{1/2}$ :  $(\infty, 0)$ ;  $(0.1, 0.1)$ ;  $(1, 1)$ ;  $(1, 2)$ ;  $(1, 10)$ . In each case, the maximum fraction of saturation activity, which we define as the saturation factor  $F_{\max}$ , is approximately reached after ten half-lives.

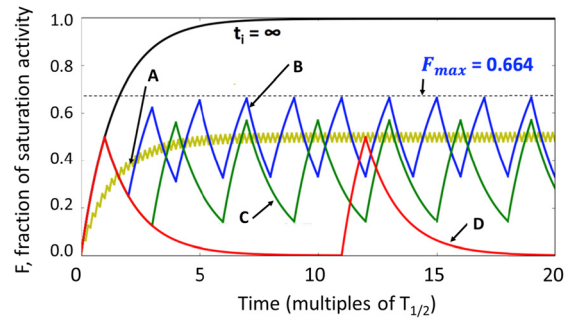


Fig. 1. Fraction of saturation activity versus time in terms of half-life ( $T_{1/2}$ ) for various  $t_i$  and  $t_d$  settings: A:  $t_i = t_d = 0.1T_{1/2}$ , B:  $t_i = t_d = T_{1/2}$ , C:  $t_i = T_{1/2}$ ,  $t_d = 2T_{1/2}$ , and D:  $t_i = T_{1/2}$ ,  $t_d = 10T_{1/2}$ .

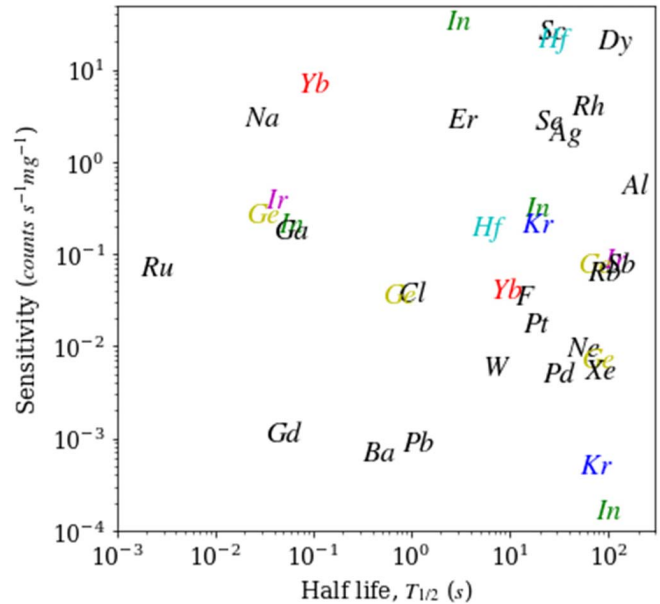


Fig. 2. Sensitivity of detection by isotope half-life, assuming  $t_i = t_d = T_{1/2}$ . Elements that have two or more activation products are shown in matching colors; otherwise, they are in black. The sensitivity is generally proportional to the product of the cross section and the detector efficiency which is energy-dependent.

$F_{\max}$  depends on both  $t_i$  and  $t_d$ . For the most convenient case of  $t_i = t_d$ , or a duty cycle of 50%,  $F_{\max} = 2/3$  [derivation omitted, but it is implicit in (6)]. For our typical PGAA geometry, based on the gamma cross section data and the detector efficiency, the sensitivity of detection for the various nuclides by their half-life is shown in Fig. 2.

The detector response to the modulated gamma emission can be derived analytically by convolving the input neutron beam pulse sequence with the production/decay response. The detector counts accumulated over the measurement time can be expressed as [7]

$$D = \varphi_0 N_0 \sigma_\gamma(E_\gamma) \varepsilon(E_\gamma) \frac{1}{\lambda} (1 - e^{-\lambda(t_i+t_r)}) \times (1 - e^{-\lambda t_d}) \left[ \frac{M}{1 - e^{-\lambda T}} - \frac{e^{-\lambda T} (1 - e^{-\lambda MT})}{(1 - e^{-\lambda T})^2} \right]. \quad (6)$$

The notations are as defined earlier, where the chopper period in the current setting is given as  $T = t_i + t_r + t_d$

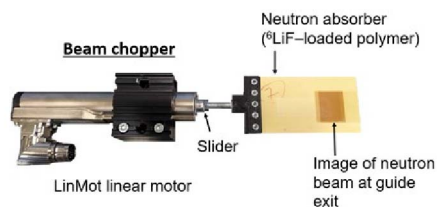


Fig. 3. Photograph of the fast shutter.  ${}^6\text{LiF}$  polymer shutter bears the imprint of the size of the neutron beam.  ${}^6\text{LiF}$  polymer was subsequently replaced by  ${}^{10}\text{B-Al}$  to eliminate the fast neutron production due to secondary reactions from thermal neutron capture by  ${}^6\text{Li}$  and to improve mechanical durability.

with the counting system's response to the chopper transition time  $t_{tr}$  included as the chopper opening time, and  $M$  is the total number of cycles.

### III. INSTRUMENTATION AND MEASUREMENT METHOD

#### A. General Instrument Configuration

The CBNA capability was developed at the PGAA instrument [11] at the National Institute of Standards and Technology Center for Neutron Research (NCNR), NIST, Gaithersburg, MD, USA. The neutron guide delivers a vertically focused beam (2 cm width  $\times$  2.7 cm height) with a neutron current of  $1.55 \times 10^{10} \text{ s}^{-1}$  approximately 40 cm upstream of the nominal sample position. The peak thermal-equivalent neutron flux on the sample is approximately  $6 \times 10^9 \text{ cm}^{-2} \cdot \text{s}^{-1}$ . A high-purity germanium detector (HPGe), surrounded by a bismuth germanate detector for Compton suppression, views the sample perpendicularly from the beam direction. The detector is interfaced to a computer-controlled digital data analyzer, Canberra Lynx\*, for either spectral or list mode data acquisition. Further information about the instrument, including the data acquisition system and shielding, can be found in [13].

#### B. Fast Shutter System

To implement CBNA for quantitative measurement of short-lived activation products, a programmable, fast linear shutter was installed at the immediate exit of the neutron guide at the PGAA station, before the connecting flight tube to the sample chamber. As shown in Fig. 3, the fast shutter consists of a purely electrical linear motor (LinMot\*) that can precisely position the slider within the stator. The linear motor is mounted on to the shield wall with a flange that also serves as a key sink. A 3-D model of the installed chopper system is shown in Fig. 4(a), and the geometry of a Monte Carlo transport simulation is shown in Fig. 4(b). A neutron-absorbing material, fastened to the end of the slider, intercepts the neutron beam in the 1.2-cm gap between the neutron guide end and the evacuated flight tube that connects to the sample chamber. This shutter was initially fabricated using a piece of  ${}^6\text{LiF}$ -loaded polymer, which has been shown to attenuate the neutron beam intensity by six orders of magnitude when it fully blocks the neutron guide exit. The  ${}^6\text{LiF}$ -loaded polymer shutter was later replaced with the  ${}^{10}\text{B}$ -loaded aluminum to eliminate fast neutron generation by  ${}^6\text{LiF}$  [14] and to improve durability.

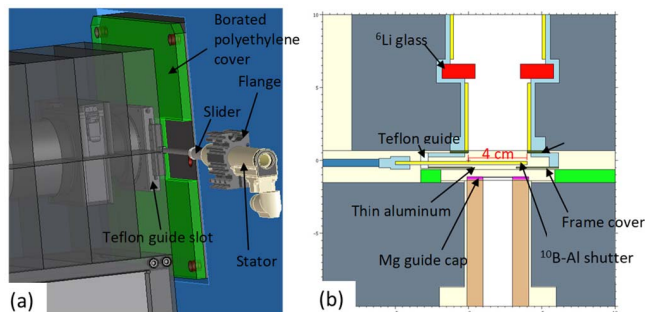


Fig. 4. (a) 3-D model showing how the linear shutter intercepts the neutron beam when it is inserted through the guide slot. (b) Geometry of the configuration of the linear shutter at the beam centerline for Monte Carlo simulation.

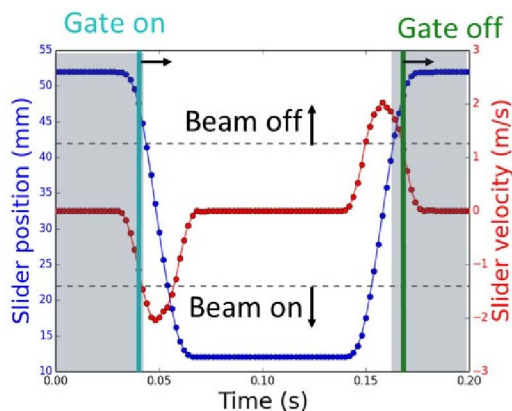


Fig. 5. Measured slider position and velocity during shutter transitions with indicated gate signals for sorting collected data.

As the neutron-absorbing shutter opens and closes, the neutron beam exiting the guide is modulated, resulting in cyclic irradiation and decay. Because the width of the guide exit is 2 cm, the travel distance of the neutron absorber was designed to be 4 cm to ensure full coverage. It is programmed such that the first and last 1 cm of travel are the acceleration/deceleration zones, so that the transitions to and from high velocities (greater than 2 m/s) are achieved with minimal torque on the motor support flange. Thus, the neutron beam is turned on or off in less than 20 ms. Fig. 5 shows the measured slider position and velocity during typical transitions in a cycle that each takes 40 ms. The gate signal, discussed in Section III.C, permits data acquisition to be collected separately for the beam ON and beam OFF phases. The dwell time following motion (i.e., the time that the beam stays ON or OFF) is specified via the LinMot software for any duration. It is possible to set zero dwell time to keep the shutter in continuous motion. Because cold neutrons, with velocities less than 2200 m/s, have finite time-of-flight on the order of milliseconds to travel from the guide end to the sample, an additional delay in the gate signal must be added to allow the neutron beam to pass through the sample to exclude possible prompt gamma rays.

#### C. Data Acquisition

Data acquisition was synchronized relative to the shutter position by configuring an output pin on the servo drive to be high (+24 V) when the slider position was less than a

programmed position and to be low (0 V) otherwise. A voltage divider circuit was used to decrease the +24-V output of the servo drive to +5 V for acceptance for the TTL of the Lynx gate input. The output signal trigger was selected when the shutter position was nearly at its end state after closing. The position was chosen to maximize the counting time when counting begins while the shutter is decelerating as it approaches its end position and counting ends, while the shutter is accelerating as it opens the neutron beam. The neutron time-of-flight was accounted for in the selected position; it was confirmed that the beam-OFF spectrum with a hydrogenous sample did not contain signal from H, which only emits prompt gamma rays.

Gamma ray spectra were acquired by three methods. In the first method, delayed and total gamma ray spectra were simultaneously acquired into separate memory groups using the combined advanced anticoincidence mode of the Lynx. Due to high variability in the detector dead time, these spectra are qualitative unless they are live-time-corrected.

This issue can be resolved by acquiring data in dual loss-free counting (DLFC) mode (method two), which corrects for live time on the fly. Because DLFC uses both memory buffers, simultaneous storage of the decay and prompt spectra is not possible, and decay and prompt spectra were measured separately.

The third method involved acquisition of the time-stamped list mode data. In addition to the aforementioned output signal trigger, an additional I/O output pin was configured to indicate the position of the shutter when the beam was completely unblocked as a result of the shutter being fully opened. The two location indicators were continuously sampled by an Arduino microcontroller using the DigitalRead function. DigitalRead returns to 0 or 1 depending on whether the voltage in the circuit is below or above 3 V, respectively. This timestamp is used to correct the timestamp in the Lynx which may have a constant offset. The time-stamped list mode data and the histogram obtained by postprocessing are illustrated in Fig. 6 for a sample containing sodium, which has an activation product, Na-22 m, with a 20-ms half-life.

#### D. Samples

Two sample mixtures were created to demonstrate capabilities with CBNA. The first mixture contained Yb and Se because the activation products have orders-of-magnitude difference in half-life: 68.2 ms for Yb-175m decay with a 514.868-keV gamma ray and 17.36 s for Se-77 decay with a 161.922-keV gamma ray. Thus, samples containing Se and Yb were chosen to demonstrate the selection of different ratios and lengths of irradiation and decay.

The second mixture contained Yb and Dy to demonstrate that the interfering signals can be resolved by discriminating the time-stamped signals into separate windows. Dy-165 has a 1.257-min half-life for decay with a 515.467-keV gamma ray, which interferes with the aforementioned 514.868-keV gamma ray from Yb-175m with a 68.2-ms half-life. Table I contains the half-lives, cross sections, and gamma ray energies for the reactions of interest.

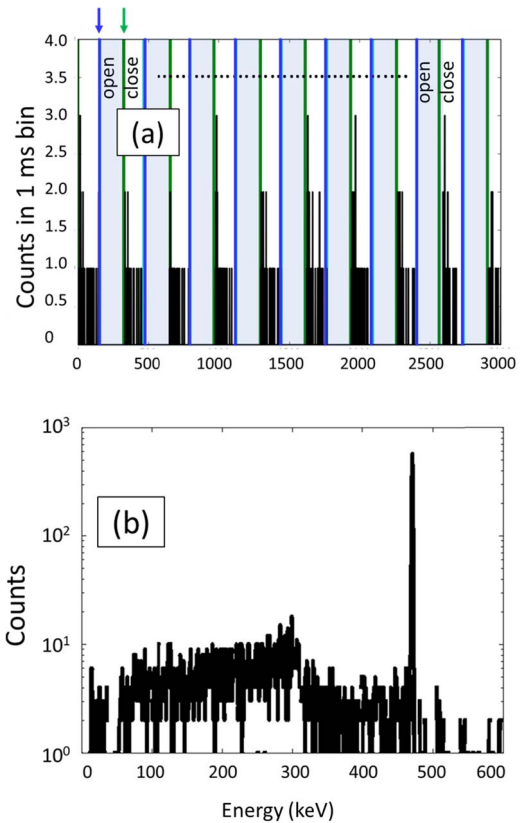


Fig. 6. (a) 3-s duration of the time-stamped list mode data acquisition recording gamma ray counts in 1-ms time bins. The position triggers are indicated by the blue and green vertical lines, respectively, corresponding to the chopper open and closed phases. (b) Gamma ray events' histogram, summed by energy bins, yielding a gamma ray spectrum in the time-integrated collection mode.

TABLE I  
HALF-LIFE AND GAMMA RAY CROSS SECTION OF SELECT ELEMENTS

Element	Yb	Dy	Se
Mixture A	0.39%	-	0.19%
Mixture B	0.60%	1.45%	-

For the two mixtures, samples were prepared in the following way: 1) mixtures of Se metal (200 mesh), Yb<sub>2</sub>O<sub>3</sub> powder, and graphite (100 mesh) and 2) mixtures of Yb<sub>2</sub>O<sub>3</sub> and Dy<sub>2</sub>O<sub>3</sub> powder and graphite (100 mesh). Mixture A was 0.19% and 0.39% mass fractions of Se and Yb, respectively; mixture B was 1.45% and 0.60% mass fractions of Dy and Yb, respectively. Each mixture was placed in a mixing mill for 30 min. Various masses of the samples were pressed into 1.3-cm-diameter pellets using a press at 44.5 kN (10 000 lb) of force. The thinner pellets (less than 200-mg mass) did not stay intact and broke into fragments, which were collected in a Teflon bag for measurement. Table II contains the mass fractions of the relevant elements in the test samples.

#### E. Measurements

Samples of mixture A with masses from about 150 to 800 mg were measured in the chopped beam with two chopper settings:  $t_i = t_d = 0.068$  s ( $T_{1/2}$  Yb-175m) and

TABLE II  
MASS FRACTIONS OF THE RELEVANT ELEMENTS CONTAINED IN THE PREPARED TEST SAMPLES

Nuclei (capture product)	<sup>175m</sup> Yb	<sup>165m</sup> Dy	<sup>165</sup> Dy	<sup>77</sup> Se
E(keV)	514.868	515.467	515.467	161.922
T <sub>1/2</sub>	0.0682 s	1.257 m	2.334 h	17.36 s
σ <sub>r</sub> (b)	9.0	6.93	0.113	0.855

TABLE III

SENSITIVITY ESTIMATED FROM MEASURED DATA (SLOPES IN FIG. 7 DIVIDED BY 900 S OF TOTAL CHOPPER OPEN TIME) FOR SE AND Yb BY CHOPPER SETTING, OPTIMIZED FOR SE AND Yb, RESPECTIVELY

Chopper settings (t <sub>i</sub> = t <sub>d</sub> = T <sub>1/2</sub> )	T <sub>1/2</sub> (Se)	T <sub>1/2</sub> (Yb)
Se (counts s <sup>-1</sup> mg <sup>-1</sup> )	3.57	2.71
Yb (counts s <sup>-1</sup> mg <sup>-1</sup> )	0.997	6.02

TABLE IV

PARAMETERS USED IN (6) TO GENERATE THE CALCULATED DETECTOR COUNTS IN TABLE V

	T <sub>1/2</sub> (S)	λ (1/s)	σ(b)	ε	t <sub>tr</sub> (s)	φ <sub>0</sub>
Se	17.36	0.03993	0.855	1	0.069 <sup>#</sup>	684.2 <sup>#</sup>
Yb	0.0682	10.16	9.00	0.5 <sup>#</sup>		

<sup>#</sup> fitting parameters for minimizing chi-squares between the calculated and the measured detector counts for all 4 chopper settings.

TABLE V

MEASURED AND CALCULATED DETECTOR COUNTS PER UNIT MASS

Chopper settings (t <sub>i</sub> = t <sub>d</sub> = T <sub>1/2</sub> )	Calculated		Measured	
	T <sub>1/2</sub> (Se)	T <sub>1/2</sub> (Yb)	T <sub>1/2</sub> (Se)	T <sub>1/2</sub> (Yb)
Se	3207.8	2456.1	3210.1	2438.5
Yb	91.036	5365.3	89.746	5415.1

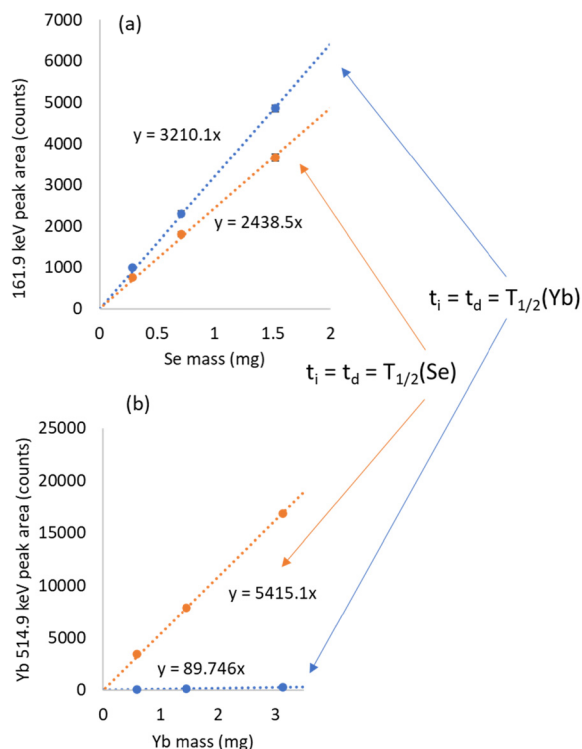


Fig. 7. Total counts of the integrated gamma peak for (a) Se and (b) Yb as a function of their respective mass, at two different settings: t<sub>i</sub> = t<sub>d</sub> = 17.36 s, optimized for Se, and t<sub>i</sub> = t<sub>d</sub> = 0.068 s, optimized for Yb. All data points were obtained with 1800 s counting time. The estimated measurement uncertainty based on counting statistics (1 standard deviation) for Se ranges from about 3% at the lowest mass to 1.5% at the highest mass. For Yb, it ranges from 1.5% to 0.75%.

t<sub>i</sub> = t<sub>d</sub> = 17.36 s (T<sub>1/2</sub> Se-77), that is, with the irradiation and decay lengths match the half-life one of the elements, thereby favoring the detection of one element over the other in the binary system. The measurement was repeated by switching the settings to favor the other element. The total measurement time was 1800 s for each setting. For mixture B, data were acquired in the list mode, for the purpose of demonstrating time discrimination for resolving overlapping peaks with a different half-life.

#### IV. RESULTS AND DISCUSSION

For the measurement using mixture A and incremented sample mass, the gamma peaks for Se (162 keV) and Yb (515 keV) were integrated and plotted against the net mass of the element, showing a linear relationship (Fig. 7), for both irradiation settings. The slope of a linear regression fit to the data corresponds to the total counts per milligram mass of the

element. Dividing the slope by the total measurement beam-on time (900 s) gives an estimate of the measured element sensitivity (counts·s<sup>-1</sup>·mg<sup>-1</sup>) for a given setting, as listed in Table III. The sensitivity is more favorable when the chopper setting is t<sub>i</sub> = t<sub>d</sub> = T<sub>1/2</sub> of the isotope of interest. The sensitivities were about 3.6 counts·s<sup>-1</sup>·mg<sup>-1</sup> for Se and about 6 counts s<sup>-1</sup>·mg<sup>-1</sup> for Yb. This is in the same order of magnitude as the estimated values of 2.5 counts·s<sup>-1</sup>·mg<sup>-1</sup> for Se and 8 counts·s<sup>-1</sup>·mg<sup>-1</sup> for Yb as shown in Fig. 2.

Using the parameters listed in Table IV and the chopper settings of t<sub>i</sub> = t<sub>d</sub> = 17.36 s, optimized for Se, and t<sub>i</sub> = t<sub>d</sub> = 0.068 s, optimized for Yb, the detector counts per unit mass can be calculated using (6), as shown in Table V. To achieve internal consistency, all four values of the measured detector counts, that is, the slopes from Fig. 7, need to agree with the calculated values. Three parameters not known exactly, namely, φ<sub>0</sub>, ε(Yb) (efficiency of the 515-keV Yb peak, relative to that for the Se peak at 162 keV), and the response to the chopper transition t<sub>tr</sub>(affecting T), have been floated for chi-square minimization to match the measured values. We note that the chopper transition should be 40 ms with microsecond precision. The longer transition time of 69 ms obtained from fitting is likely due to the approximation of a full irradiation while the chopper is in transit, as treated in (6). This uncertainty is entirely negligible with half-lives in the tens of seconds such as Se. However, it plays a more important role for the very short-lived isotopes such as Yb-175m. The relative efficiency of about 0.50 at the Yb peak is not unreasonable compared with the detector calibration value of 0.56. φ<sub>0</sub> represents the neutron flux for the given

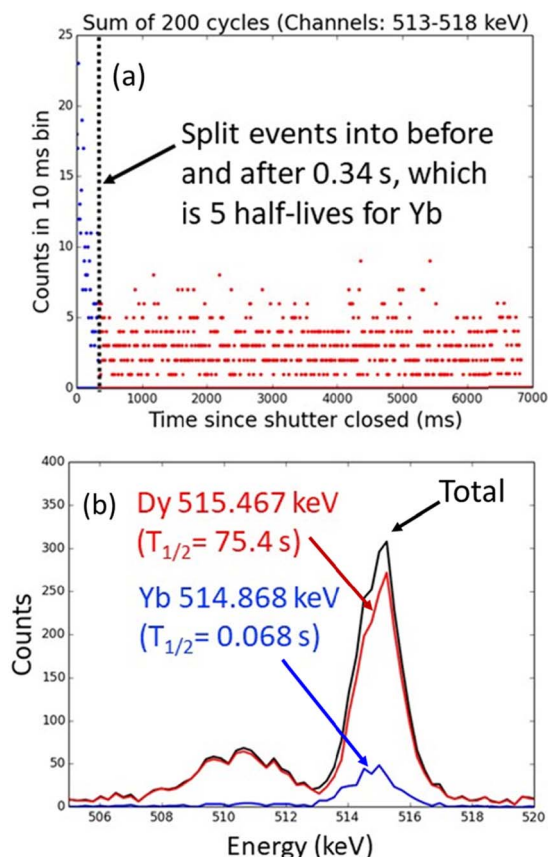


Fig. 8. (a) Postprocessing of time-stamped list mode data binning counts by time relevant to each decay half-life to accentuate the element of interest. The counts that arrived before 0.34 s are mainly due to the shorter lived Yb ( $T_{1/2} = 0.068$  s), whereas the rest is attributed to Dy ( $T_{1/2} = 75.4$  s). (b) Normal spectrum in the histogram mode would not have resolved the overlapping peaks. The blue peak corresponds to the events in the short time window before 0.34 s, and the red peak is from the rest of the time window.

geometry, which is in common for Se and Yb and therefore is just a normalization constant. The difference between the measured and calculated detector counts is less than 1.5% for all four counts.

Additional information contained in the list mode data can be extracted by postprocessing. For example, by discriminating the event timing, the shorter lived peak can be separated from the longer lived one, as in the case of Yb ( $T_{1/2} = 0.068$  s) and Dy ( $T_{1/2} = 75.4$  s), as shown in Fig. 8. This particular example demonstrates the separation of overlapping peaks—both peaks are close to 515 keV and cannot be resolved even with the high-resolution HPGe detector in the normal histogram mode but can be time-resolved by their half-lives in the list mode.

## V. CONCLUSION

We have demonstrated CBNA based on a linear neutron beam chopper system, which enables in-beam neutron activation analysis for short-lived isotopes without the need for sample transfer as in traditional INAA. Limited only by a short (40 ms) chopper transition time, CBNA could allow NAA access to the short-lived isotopes such as those shown in Fig. 2 that are challenging for traditional INAA. The test samples of incremental masses comprising Se-77 ( $T_{1/2} = 17.36$  s) and Yb-175m ( $T_{1/2} = 0.0682$  s) were

measured with the chopper timing optimized for each isotope, showing a higher sensitivity when the irradiation and counting times match the half-life of the isotope of interest. The measurements demonstrated the feasibility of using CBNA for quantitative analysis. Consistent results were obtained for theoretical calculations of the detector response, with proper normalization and a chopper transition time. A test sample containing Yb-175m and Dy-165 ( $T_{1/2} = 75.4$  s) was measured using list mode data acquisition, enabling the separation of overlapping energy peaks by time gating. Future applications of this chopper system to other short-lived isotopes are planned.

## ACKNOWLEDGMENT

The authors acknowledge their late colleague Rolf Zeisler for his inspirations and enthusiastic support for this project. This work was performed while Danyal J. Turkoglu held an NRC Research Associateship Award at NIST, Gaithersburg, MD, USA. The NCNR Research Facility Operations Group, NIST, contributed to technical assistance of the chopper design and fabrication process.

## REFERENCES

- [1] W. W. Givens, W. R. Mills, and R. L. Caldwell, "Cyclic activation analysis," *Nucl. Instrum. Methods*, vol. 80, no. 1, pp. 95–103, Apr. 1970.
- [2] A. Chatt, K. N. Desilva, J. Holzbecher, D. C. Stuart, R. E. Tout, and D. E. Ryan, "Cyclic neutron activation analysis of biological and metallurgical samples," *Can. J. Chem.*, vol. 59, no. 11, pp. 1660–1664, Jun. 1981.
- [3] T.-P. Cheng, J. S. Morris, S. R. Koirtyohann, V. L. Spate, and C. K. Baskett, "The analysis of human nails for 24 elements via k0 and cyclic neutron activation analysis," *Nucl. Instrum. Methods Phys. Res. A, Accel. Spectrom. Detect. Assoc. Equip.*, vol. 353, nos. 1–3, pp. 457–460, Dec. 1994.
- [4] A. Egan, S. A. Kerr, and M. J. Minski, "Determination of selenium in biological materials using sup (77 m) Se ( $T = 17.5$  sec) and cyclic activation analysis," *Radiochem. Radioanal. Lett.*, vol. 28, nos. 5–6, pp. 369–378, 1977.
- [5] R. E. Tout and A. Chatt, "The effect of sample matrix on selection of optimum timing parameters in cyclic neutron activation analysis," *Analytica Chim. Acta*, vol. 133, no. 3, pp. 409–419, Sep. 1981.
- [6] A. S. Farooqi, W. Arshed, O. A. Akanle, C. Jaynes, and N. M. Spyrou, "Fluorine determination in diet samples using cyclic INAA and PIGE analysis," *J. Radioanal. Nucl. Chem. Articles*, vol. 161, no. 1, pp. 71–78, Aug. 1992.
- [7] N. M. Spyrou, "Cyclic activation analysis—A review," *J. Radioanal. Chem.*, vol. 61, nos. 1–2, pp. 211–242, Mar. 1981.
- [8] R. M. Lindstrom and Z. Révay, "Prompt gamma neutron activation analysis (PGAA): Recent developments and applications," *J. Radioanal. Nucl. Chem.*, vol. 314, no. 2, pp. 843–858, Nov. 2017.
- [9] R. Zeisler, G. P. Lamaze, and H. H. Chen-Mayer, "Coincidence and anti-coincidence measurements in prompt gamma neutron activation analysis with pulsed cold neutron beams," *J. Radioanal. Nucl. Chem.*, vol. 248, no. 1, pp. 35–38, 2001.
- [10] G. L. Molnár, "Prompt gamma activation analysis using a chopped neutron beam," *J. Radioanal. Nucl. Chem.*, vol. 264, no. 2, pp. 277–281, May 2005.
- [11] L. Szentmiklósi, Z. Révay, and T. Belgya, "An improved beam chopper setup at the Budapest PGAA facility," *Nucl. Instrum. Methods Phys. Res. B, Beam Interact. Mater. At.*, vol. 263, no. 1, pp. 90–94, Oct. 2007.
- [12] L. Szentmiklósi, T. Belgya, Z. Révay, and Z. Kis, "Upgrade of the prompt gamma activation analysis and the neutron-induced prompt gamma spectroscopy facilities at the Budapest research reactor," *J. Radioanal. Nucl. Chem.*, vol. 286, no. 2, pp. 501–505, Nov. 2010.
- [13] D. Turkoglu, H. Chen-Mayer, R. Paul, and R. Zeisler, "Assessment of PGAA capability for low-level measurements of H in Ti alloys," *Analyst*, vol. 142, no. 20, pp. 3822–3829, 2017.
- [14] D. Turkoglu, R. G. Downing, W. Chen, D. Sahin, and J. Cook, "A  $^3\text{He}$  beam stop for minimizing gamma-ray and fast-neutron background," *J. Radioanal. Nucl. Chem.*, vol. 311, no. 2, pp. 1243–1249, Feb. 2017.